Published in final edited form as:
J Am Coll Cardiol. 2012 February 7; 59(6): 616–626. doi:10.1016/j.jacc.2011.10.881.

In Vivo Detection of Oxidation-Specific Epitopes in Atherosclerotic Lesions Using Bio-Compatible Mn(II) Molecular Magnetic Imaging Probes

Karen C. Briley-Saebo, PhD[*,#], **Tuyen Hoang**[*], **Alexander M. Saeboe**[*], **Young Seok Cho, MD**[‡,+], **Sung Kee Ryu, MD, PhD**[+,¥], **Eugenia Volkava**[*], **Stephen Dickson, MS**[*], **Gregor Leibundgut, MD**[+,&], **Philipp Weisner, MD**[&], **Simone Green, BS**[+], **Florence Casanada, BS**[+], **Yury I. Miller, MD, PhD**[&], **Walter Shaw, PhD**[@], **Joseph L Witztum, MD**[&], **Zahi A. Fayad, PhD**[*,§], and **Sotirios Tsimikas, MD**[+]

[*]Imaging Science Laboratory, Department of Radiology, Mount Sinai School of Medicine, New York, New York

[#]Department of Gene and Cell Medicine, Mount Sinai School of Medicine, New York, New York

[+]Vascular Medicine Program, University of California San Diego, La Jolla, California

[&]Department of Medicine, University of California San Diego, La Jolla, California

[‡]Seoul National University, South Korea

[¥]Eulji University, Seoul, South Korea

[§]Departments of Cardiology, Zena and Michael A. Weiner Cardiovascular Institute and Marie-Josee and Henry R. Kravis Cardiovascular health Center, Mount Sinai School of Medicine, New York, New York

[@]Avanti Polar Lipids, Alabaster, AL

Abstract

Objectives—To evaluate the in vivo magnetic resonance (MR) imaging efficacy of manganese (Mn(II)) molecular imaging probes targeted to oxidation-specific epitopes (OSE).

Background—OSE are critical in the initiation, progression and de-stabilization of atherosclerotic plaques. Gadolinium (Gd(III)) based MR imaging agents can be associated with systemic toxicity. Mn is an endogenous, bio-compatible, paramagnetic metal ion that has poor MR efficacy when chelated, but strong efficacy when released within cells.

Methods—Multimodal Mn-micelles were generated to contain rhodamine for confocal microscopy and conjugated with either the murine monoclonal IgG antibody MDA2 targeted to malondialdehyde (MDA)-lysine epitopes or the human single-chain Fv antibody fragment IK17

Address for Correspondence: Karen C. Briley-Saebo, saebo@mountsinai.org or Sotirios Tsimikas, UCSD, Cardiology, 9500 Gilman Drive, BSB 1080, La Jolla, CA 92093-0682, USA, (858) 534-6109, (858) 534-2005 (fax), stsimikas@ucsd.edu, stsimikas@ucsd.edu.

Disclosures

Dr Tsimikas and Witztum are co-inventor of patents, owned by the University of California, on the potential clinical use of antibodies MDA2 and IK17 and have equity interest in Atherotope, Inc. Drs Fayad and Briley-Saebo are consultants to Atherotope, Inc.

targeted to MDA-like epitopes ('targeted micelles"). Micelle formulations were characterized in vitro and in vivo and their MR efficacy (9.4 Tesla) evaluated in apoE$^{-/-}$ and LDLR$^{-/-}$ mice (0.05 mmol Mn/Kg dose) (total of 120 mice for all experiments). In vivo competitive inhibition studies were performed to evaluate target specificity. Untargeted, MDA2-Gd and IK17-Gd micelles (0.075 mmol Gd/Kg) were included as controls.

Results—In vitro studies demonstrated that targeted Mn-micelles accumulate in macrophages when pre-exposed to MDA-LDL with ~10X increase in longitudinal relativity. Following intravenous injection, strong MR signal enhancement was observed 48–72 hours after administration of targeted Mn-micelles, with co-localization within intraplaque macrophages. Co-injection of free MDA2 with the MDA2-Mn micelles resulted in full suppression of MR signal in the arterial wall confirming target specificity. Similar MR efficacy was noted in apoE$^{-/-}$ and LDLR$^{-/-}$ mice with aortic atherosclerosis. No significant differences in MR efficacy were noted between targeted Mn and Gd micelles.

Conclusions—This study demonstrates that bio-compatible multimodal Mn-based molecular imaging probes detect OSE within atherosclerotic plaques and may facilitate clinical translation of non-invasive imaging of human atherosclerosis.

Keywords

Atherosclerosis; MRI; oxidation; molecular imaging; inflammation

Introduction

Oxidized low density lipoproteins (OxLDL) have been identified as one of the main factors in the initiation, progression, and de-stabilization of atherosclerotic plaques(1–4). The presence of "oxidation-specific epitopes" (OSE) within the arterial wall initiates the recruitment and activation of monocytes thereby promoting macrophage accumulation. Once activated, intraplaque macrophages take up OxLDL in an unregulated fashion forming foam cells that are retained in the arterial wall. Apoptosis and necrosis of foam cells amplifies chronic inflammatory responses and eventually leads to plaque rupture.

Since OxLDL is immunogenic, murine and human monoclonal antibodies that bind unique OSE can be generated and have been identified, characterized and purified and shown to bind to murine and human atherosclerotic plaques. Recently we have reported the use of oxidation-specific antibody(MDA2, E06, and IK17)-labeled gadolinium (Gd) micelles and iron oxide nanoparticles for the in vivo detection of OSE in atherosclerotic lesions of apoE$^{-/-}$ mice using MR imaging(5,6) and showed that these nanoparticles accumulate within intraplaque macrophages. In vitro cell studies strongly suggested that uptake is specific and receptor mediated and relies upon interaction of the targeted nanoparticle with endogenous OxLDL. Once taken up by macrophages, the entire lipid nanoparticle is metabolized within intracellular vesicles (lysosomes/endosomes). Although chelated Gd is renally excreted (>99.9%) bio-retention and in vivo biotransformation of Gd(III) micelles was observed due to their prolonged half-life. This may lead to systemic toxicity in renally impaired patients(7–9).

Manganese (Mn(II)) is an endogenous paramagnetic metal that has been used in other FDA approved contrast agents for hepatocyte targeting and MR liver indications(10,11). Although biocompatible, Mn is typically not used in MR contrast agent development due to its low magnetic moment that limits MR signal enhancement relative to Gd. However, studies have indicated that if Mn is delivered into a cell, interaction with intracellular components and metalloproteinase results in significant (>20 fold) increases in MR efficacy (Figure 1) (12–14). Based on prior studies with targeted Gd-micelles, we hypothesized that it may be

possible to produce Mn probes that exhibit limited MR efficacy in the vascular phase where the Mn remains completely chelated but high MR efficacy once Mn is released within intraplaque macrophages and foam cells. The intracellular release of Mn would enhance the MR signal by both increasing the number of water exchange sites (q>0) and by decreasing the molecular tumbling rates due to interaction with macromolecules and cell membranes. Chelation in the vascular phase has two significant effects: 1) reduces potential cardiotoxicity associated with bolus injection of free Mn (MnCl2) and 2) background signal from blood is nominal since there are no inner sphere water exchange sites available (q=0) if DTPA is used as the chelating agent. The antibody associated with the surface of the particle allows for binding of the micelle to endogenous OSE found in circulation and/or within the arterial wall (5,6). The Mn micelle-Ab-OxLDL complex is then taken up by intraplaque foam cells/macrophages, as shown with Gd-micelles. This degradation would result in the intracellular release of the Mn metal ions that are then either taken up by metalloproteinase or interact with the cell membrane.

The aim of the current study was therefore to synthesize, characterize, and evaluate the MR efficacy of targeted Mn molecular imaging probes to OSE in murine models of atherosclerosis and to compare their imaging properties to previously described Gd targeted probes (5).

Abbreviated Materials and Methods (Please see full details in Online Supplement)

Antibodies and Micelle synthesis

MDA2 is a murine IgG monoclonal antibody that binds malondialdehyde (MDA)-lysine epitopes present on OxLDL(15,16). IK17 is a human single chain Fv fragment (scFv) that recognizes an MDA-related epitope expressed on both MDA-LDL and copper oxidized LDL. The following micelle formualations were prepared: untargeted Mn and Gd micelles, MDA2-Mn and Gd micelles and scFv IK17-Mn micelles.

Characterization

All micelle formulations were characterized with respect to particle size, zeta potential, Mn or Gd content, in vitro MR efficacy, vascular stability, and uptake by J447A.1 murine macrophages. Relaxometry was used to evaluate transmetallation of the Mn and Gd from untargeted formulations to other proteins in human plasma.

Animal Models

All mice used in the current study are summarized in Table 1.

Neurotoxicity

Since studies have shown that high repeat i.v administration of $MnCl_2$ may lead to neurotoxicity, the uptake of the PEG micelles was evaluated in murine models of Alzheimer's disease(17). This model was chosen as studies have shown significant OSE deposition in the lesions of these mice(18)). Due to the high endogenous concentration of Mn, dysprosium (Dy) micelles were prepared as described above (DyDTPA- bis(stearyl-amid) was provided by Avanti Polar lipids). It should be noted that due to the high electronic relaxation rate and susceptibility of Dy, uptake of Dy into tissue results in MR signal loss (19)). Mice were injected with 0.075 mmol Dy/Kg of either untargeted (n=3) or MDA2 labeled (n=3) Dy micelles. MR imaging was performed prior to injection and over a 72-hour time interval post injection. Immediately following the last scan, mice were sacrificed, saline

perfused and the brain excised, cleaned and weighed. The concentration of Dy (per gram wet weight) was then determined using ICP-MS.

In vivo MR Imaging

All in vivo MR imaging was performed at 9.4T (400 MHz, Bruker Instruments, Billerica, MA), using previously reported methodology(5,6). In short, all animals underwent a pre-injection MR scan within 24 hours prior to the administration of the various micelle formulations. MR imaging was performed over a 1-week time interval after tail vein injection of either a 0.050 mmol Mn/Kg dose or a 0.075 mmol Gd/Kg dose of micelles. MR imaging of the abdominal aorta was performed using a T1-weighted black blood spin-echo sequence (TR/TE/flip = 800 ms/8.6 ms/30°, NEX=16, FOV=2.6 cm×2.6 cm) with a micro-scale in-plane resolution of 0.098 mm^2. In order to quantitatively evaluate the MR data, signal intensity (SI) measurements were obtained using regions of interest (ROIs) within the aortic wall on slices (n>3) exhibiting signal modulation post contrast using ImageJ software. SI measurements of adjacent muscle and the standard deviation associated with noise were also obtained for each slice. The percent-normalized enhancement (%NENH), relative to muscle, was then determined for the aortic vessel wall and liver according to established methods(5). The %NENH values reflect the percent relative change in the contrast to noise ratios (CNR) as a function of time post injection. For neuro imaging, T2-weighted spin echo sequences were used (TR/TE=125 ms/18 ms, NEX=8, FOV=2.6 cm×2.6 cm, 12 slices). The anatomy of the brain was used to match the images pre and post injection. Signal intensity (SI) measurements were obtained using ROIs within the cerebellum, cerebrum and locations exhibiting lesion deposition (slices>2). The percent-normalized enhancement (%NENH), relative to muscle, was then determined.

Confocal Microscopy

To evaluate J774A.1 macrophage uptake or co-localization of the rhodamine labeled micelles within the arterial wall, confocal microscopy was performed as reported previously (5).

In Vivo Competitive Inhibition Studies

The specificity of the MDA2-Mn micelles for MDA-lysine epitopes within the vessel wall of apoE−/− mice was evaluated using in vivo competitive inhibition, as previously described(5,6).

immunohistochemistry

MDA epitopes detected using purified guinea pig antiserum MDA3 (1:500 dilution), as described previously(6,15).

RESULTS

Physical properties, relaxivities and half-life of the various micelle formulations

The micelle formulations were 10–22 nm in size (Table 2), similar to other PEG-DSPE based micelles(5,20). The smaller hydrated particle size observed for Mn micelles relative to Gd was likely due to limited water co-ordination associated with the q=0 Mn formulations. The addition of the antibodies resulted in an increase in the mean hydrated particle size of all formulations tested. Due to the higher magnetic moment, as well as the ability to coordinate water protons within the innersphere (q=1 for GdDTPA), all Gd formulations exhibited significantly greater r1 values in HEPES buffer relative to equivalent Mn micelles(21). The r1 values observed for the Mn micelles were, however, higher than those expected for q=0 complexes(21). The elevated r1 values are likely caused by an added

second sphere contribution due to the presence of uncoordinated carboxylic groups. All antibody labeled micelles exhibited increased r1 values when analyzed in apoE−/− mice blood, relative to values measured in WT mouse blood (Table 2). The intracellular r1 values obtained for MDA2-Mn micelles (45.5±5 $s^{-1}nM^{-1}$) which were pre-incubated with MDA-LDL in J744A.1 macrophages was significantly greater than the values obtained in either HEPES buffer (4.1±0.2 $s^{-1}nM^{-1}$) or apoE−/− mouse blood (8.1±0.4 $s^{-1}nM^{-1}$). No significant intracellular r1 values were observed for untargeted Mn micelles thereby suggesting limited intracellular uptake of the untargeted formulation. The surface charge, as defined by the zeta potential, was significantly greater for Gd versus micelles (−6±1 vs. −4 ± 1 mV, $p<0.01$).

Vascular Stability

Untargeted Gd micelles show no significant change in the r1 values after 24 hours incubation but did show an initial increase in the r1 values in plasma (time < 5minutes) relative to buffer (r1=14 $s^{-1}mM^{-1}$ versus 10.4 $s^{-1}mM^{-1}$, $p<0.01$). This may be indicative of an initial and potentially rapid transmetallation that occurs within 5 minutes post incubation. For the untargeted Mn micelles, the r1 values decreased by 6% over the 24 hour time period studied (3.75 $s^{-1}mM^{-1}$ versus 3.50 $s^{-1}mM^{-1}$). The initial r1 values in plasma were not significantly different than those observed in buffer, indicating slower kinetics of the transmetallation relative to Gd.

The IK17-Gd and IK17-Mn micelles exhibited 3.5% and 1.5% transmetallation after incubation with 20 μmol/l zinc and copper, respectively, suggesting that both the Gd and Mn formulations are susceptible to in vivo transmetallation with endogenous metal ions (Figure 2).

Macrophage uptake of antibody-micelle formulations

Significant cell association (binding and/or uptake) of IK17-Mn by J774A.1 macrophages pre-exposed to MDA-LDL was noted (Figure 3). Only limited unspecific uptake was observed for the untargeted micelles. These results are consistent with previously reported results that show specific uptake of OxLDL targeted Gd micelles by in vitro macrophages(6).

Pharmacokinetics and Biodistribution

Targeted (with both MDA2 and IK17) Mn and Gd micelles had significantly longer (5–10X) circulating half-life lives than untargeted micelles in apoE−/− mice (Table 2). The endogenous background concentration of Mn in apoE−/− mouse blood was 0.32 ± 0.05 μg/ml. Multi-exponential decay was observed for all Mn formulations thereby suggesting re-circulation of metabolized Mn. Additionally, the variation observed in the pKa between the Mn and Gd micelles is likely due to differences in dose or number of particles injected (0.05 mmol Mn/Kg and 0.075 mmol Gd/Kg) as well as differences in surface charge (zeta potential) associated with the particles (−4 mV for Mn micelles and −6 mV for Gd micelles).

The biodistribution of untargeted and MDA2-Mn micelles in the liver, kidney, and aorta are shown in Figure 4. Compared to MDA2-Gd micelles, significantly higher uptake (per gram wet weight) of MDA2-Mn micelles was observed within the aorta and significantly lower uptake in the liver 24-hour post injection. Untargeted micelles exhibited limited uptake in the arterial wall. Whereas the excretion kinetics of MDA2-Gd out of the arterial wall was complex, the elimination of MDA2-Mn micelles was mono-exponential with an elimination half-life of 58.7 hours and all Mn was eliminated out of the kidneys within 168 hours post injection. Residual kidney uptake (0.97% ID) was observed for the MDA2-Gd micelles at 1-

week post injection. No significant uptake (<0.05%) of untargeted or MDA2-Mn micelles was observed in the following tissue at any of the time points tested: lung, bone, and heart. At 24 hours post injection, approximately 0.1% of the MDA2 labeled Mn(II) formulation was present within the spleen. MDA2-Gd micelles, however, exhibited significant uptake in the lung (0.47% ID), heart (0.35% ID), bone (0.17% ID) and spleen (6.27% ID) at 48 hours post injection.

The initial lower uptake of Mn micelles within the liver, spleen and kidney is likely a function of dose (lower concentration of Mn micelles injected relative to Gd micelles). However, the higher uptake of targeted Mn micelles within the arterial wall may be related to charge that may influence the binding of the targeted particles to endogenous OSE. Variations in the excretion kinetics, however, are likely related to the rate of intracellular metabolism of Mn and Gd.

Neurotoxicity

No significant ($p>0.1$) change in the MR signal intensity was observed in the brain of Alzheimer's mice after administration of either untargeted or targeted micelles. Additionally, all ex vivo Dy tissue concentrations determined by ICP-MS were below method detection limits. As a result, the Dy concentration within the brain could not be accurately determined. Based upon these findings it is evident that the PEG micelles are unable to cross the intact bold brain barrier (BBB).

In vivo MR Imaging

Serial imaging was performed at baseline and at 24, 48, 72, 96 hours and 1-week post injected of targeted micelles. Significant and robust MR signal enhancement was observed in the arterial wall of apoE$^{-/-}$ mice following administration of a 0.05 mmol Mn/kg dose of MDA2-Mn and IK17-Mn micelles (Figure 5), relative to untargeted formulations. Maximum signal enhancement was observed 48–72 hours after administration of the OxLDL targeted Mn micelles. Quantitatively, MDA2 and IK17-Mn micelles exhibited 141±20% and 125±6% ($p<0.001$ for each compared to pre-injection values) higher signal than adjacent muscle at 48 hours post injection. Additionally, MR signal enhancement of 124±7% was observed in LDLR$^{-/-}$ mice 48 hours after administration of MDA2-Mn micelles (Figure 6). Although the mean values were lower in LDLR$^{-/-}$ mice, no statistically significant difference was observed between the apoE$^{-/-}$ and LDLR$^{-/-}$ mice. In vivo competitive inhibition studies in apoE−/− mice showed a 92% ($P<0.001$) reduction in MR signal for mice administered free MDA2 at the time of MDA2-Mn micelle injection.

MR imaging of the MDA2-Gd micelles showed maximum signal occurring (%NENH=156±21%) at 1 week after the administration of a 0.075 mmol Gd/Kg dose (Figure 7). The results obtained in the current study were similar to those reported for 12–13 month old apoE−/− mice following administration of MDA2-Gd micelles(5). No significant difference in the MR efficacy was observed between the MDA2-Mn and MDA2-Gd micelles at the optimal imaging time points post injection (48 hours versus 1 week, respectively).

Plaque macrophage uptake of targeted micelles

Confocal microscopy confirmed the uptake of MDA2-Mn micelles within atherosclerotic lesions and specifically within intraplaque foam cells 48 hours post injection (Figure 8). Rhodamine labeled targeted micelles were not observed in the extracellular matrix. Additionally, rhodamine was not present within the arterial wall after 1-week post injection. These results are consistent with the findings reported for MDA2-Gd micelles(5). For the untargeted Mn micelles, no significant rhodamine signal was observed within the arterial

wall at any of the time points tested. MDA epitopes were present in regions exhibiting plaque deposition and signal enhancement by MRI (Figure 9), consistent with histological findings from prior radionuclide imaging studies using the same targeting antibodies (15,16).

DISCUSSION

This study demonstrates the novel development of Mn based MR molecular imaging probes and their successful application of serial, non-invasive imaging of atherosclerotic plaques in two murine models of atherosclerosis. These multimodal micelles are composed of an optical tag, the Mn for MR imaging and oxidation-specific antibodies to enhance specific targeting of atherosclerotic lesions. Importantly, although MnDTPA based probes theoretically exhibit less MR efficacy than equivalent GdDTPA probes, these specifically designed Mn probes accumulated within intraplaque macrophages, presumably due to binding of extracellular OxLDL in the vessel wall or plasma and subsequent uptake in macrophages through scavenger receptors. The intracellular accumulation of targeted Mn-micelles and de-metallation resulting in free Mn, noted both in vitro and in vivo, resulted in significant increases in intracellular r1 values, enhanced MR efficacy, and effective imaging of atherosclerotic lesions. Furthermore, specific targeting of OSE was demonstrated by the fact that untargeted control micelles provided limited lesion enhancement and that co-treatment of animals with free MDA2 and MDA2-Mn micelles showing markedly reduced MR signal enhancement due to blocking of available antibody binding sites. Since Mn is a relatively non-toxic cation and non-cardiovascular formulations are FDA approved, these data provide a framework for the clinical translation of this approach to imaging human atherosclerosis and vulnerable plaques.

Mn is a paramagnetic endogenous metal ion that is considered safe when chelated during the bolus injection(22,23). Chelation of Mn during the bolus is critical in order to eliminate cardiotoxicity caused by the competition of Mn ions with calcium in normal cardiomyocytes. However, studies have shown that even soluble Mn (as $MnCl_2$) is safe if it is administered as a slow infusion(24). In the current study, DTPA was used to chelate Mn in the vascular phase. Although limited vascular transmetallation was observed, the kinetics associated with the vascular release of Mn was relatively slow (>5 minutes). These findings are consistent with reported MnDTPA-BMA data that show relatively slow kinetics with transmetallation half-lives in human plasma of greater than two minutes (non-first order kinetics)(25). Reported studies using similar GdDTPA lipid micelle constructs have shown 1.6% transmetallation of Gd three hours after injection in mice(26). Although minor vascular transmetallation is observed with the Mn micelle formulations, toxicity issues caused by the bio-transformation and bio-retention of Mn chelates are minimal compared to that of equivalent Gd formulations(7,27). Additionally, since the PEG micelles are unable to cross the intact BBB, issues related to neurotoxicity are expected to be nominal. The small concentration of Mn that may transmetallate in the vascular phase is also not expected to induce neurotoxicity. Reported toxicity studies using FDA approved MnDPDP (Telsascan) that undergoes 20% transmetallation in the vascular phase does not induce clinical signs indicative of neurotoxicity (28).

Studies have shown that most cells quickly metabolize or utilize soluble Mn either via integration into Mn specific metalloproteins or interaction with other cellular components such as the cell membrane(12,13). The in vivo biodistribution data showed 97% clearance of the MDA2-Mn micelles within 1-week post injection. The MDA2-Gd micelles, however, exhibited only 72.9% clearance within 1-week post injection. The variation in the retention is due to differences in the rate of metabolism of Mn and Gd micelles. For example, confocal studies show that the targeted PEG micelles were completely degraded within

intraplaque macrophages 72 hours after injection (rhodamine signal is no longer present). However, as confirmed by ICP-MS as well as MRI, Gd is still present within the arterial wall. These data illustrate that the targeted micelles and Gd or Mn label track together at early time points post injection (<72 hours). However, as the intraplaque macrophages internalize and degrade the particles, the lipids forming the micelles and MR label are no longer co-localized within the arterial wall. During intracellular metabolism the cells degrade the particles and the MR label is released from the chelate. For targeted Mn micelles, the Mn interacts with cellular components and eventually is either exocytosed or integrated into the endogenous Mn pool. However, de-metallation of Gd results in the formation of insoluble Gd salts that remains within the intracellular vesicles (8). So whereas the half-life of Mn within the arterial wall was approximately 60 hours (or 2.5 days), MDA2-Gd micelles exhibit prolonged retention of Gd (>1 week).

The results of the current study strongly indicate that the novel Mn probes allow for specific delivery of Mn to the target cells such as macrophages. This was demonstrated by several lines of evidence: 1- the strong MR signal enhancement observed within the arterial wall 48–72 hours post MDA2 or IK17 Mn micelles injection. Strong signal enhancement may only be observed after intracellular de-metallation of Mn; 2- Consistent with specific targeting mechanisms, pre-injection with free MDA2 resulted in complete MR signal inhibition of MDA2-Mn micelles. If passive unspecific uptake mechanisms were present, then the addition of excess free MDA2 would not limit uptake into intraplaque macrophages and the MR signal would not be affected; 3- confocal microscopy confirmed uptake of the micelles within intraplaque macrophages and the presence of MDA epitopes; and 4- the fact that the MR signal and rhodamine signal returned to baseline within one week post injection is indicative that the intraplaque macrophages/foam cells are able to effectively degrade and clear the de-metallated Mn and lipid fragments within a relatively short time period post injection. The molecular mechanisms through which targeted micelles accumulate in macrophages after being exposed to OxLDL are actively being investigated and may be mediated through macrophage scavenger receptors, macropinocytosis or other mechanisms. Future studies are underway to fully define the mechanism of intracellular uptake.

This study significantly advances the approach of targeting OSE for molecular imaging of atherosclerotic lesions non-invasively by providing both a more easily translatable approach and higher specificity for targeting OxLDL-enriched macrophages. Prior studies using radiolabeled oxidation-specific antibodies have shown that their uptake in mouse and rabbit atherosclerotic lesions is strongly correlated with plaque burden, measured both as percent atherosclerosis surface area and aortic weight(15,16,29). Furthermore, in dietary regression studies it was demonstrated that reduced plaque uptake of radiolabeled antibodies was highly sensitive to regression of atherosclerosis and removal of OSE (29). In fact, areas within the aorta where the loss of OSE was greatest were characterized by phenotypes of plaque stabilization, such as absence of OxLDL and macrophages and accumulation of smooth muscle cells and collagen. Furthermore, in rabbits with very advanced plaques containing fibrous lesions, there was also evidence of reduced OxLDL content and antibody accumulation. If these results can be confirmed in patients, one would be able to quantitate the burden of OSE and monitor their regression.

We have recently reported that targeted Gd-micelles may be used to accurately identify OSE within the arterial wall of apoE−/− mice using high resolution MRI(5). We have validated and significantly extended these observations by performing comparative studies of transmetallation, serial pharmacokinetics, biodistribution and imaging to 1 week with both Gd and Mn IK17-micelles and MDA2-miceles in age matched LDLR−/− and apoE−/− mice. Although MDA2-Mn micelles were administered at dose that was 33% lower than that of Gd, equivalent MR signal enhancement was observed at the optimal imaging time points

post injection. For targeted Mn micelles, maximum signal enhancement was observed 48–72 hours post injection with no significant signal observed after 1 week. MDA2-Gd micelles, however, exhibited maximum enhancement after 1-week post injection. However, like all lipid based nanoparticles, a fraction of the injection dose was sequestered by liver causing bio-retention of Mn and Gd(5). Unlike with targeted Mn-micelles, Gd remains in the plaque for at least a week. Reported studies indicate that intracellular uptake of Gd may promote cell apoptosis, which may result in pro-inflammatory effects(8,30). However, the intracellular toxicity is strongly dependent upon intracellular uptake into vesicles (endosomes/lysosomes) and the formation of toxic insoluble Gd salts. Liver uptake of Mn, however, is not toxic and Mn based targeted liver agents have been approved by the FDA(11).

To avoid potential toxic effects of free Gd, we have also successfully imaged atherosclerotic lesion in apoE−/− mice with MDA2, IK17 and E06 targeted lipid coated ultra-small superparamagnetic iron oxide particles(31). Once taken up by macrophages, iron oxide particles generate MR signal loss due to the generation of strong T2/T2* effects. This approach is qualitatively different than using untargeted iron oxide based nanoparticles that non-specifically accumulate in intraplaque macrophages(32,33). A recent therapeutic study in patients showed a significant change in MR signal after 6–12 weeks high dose atorvastatin treatment (relative to baseline T2* values), and it is anticipated that targeted iron oxide nanoparticles will enable specific detection and monitoring high risk atherosclerotic plaque(31,32).

The clinical relevance of OSE targeted imaging shown in the current study was recently demonstrated in coronary sections from sudden death victims where the presence of OxPL and IK17 epitopes was strongest in late lesions with macrophage-rich areas, lipid pools and the necrotic core and were most specifically associated with unstable and ruptured plaque. This was further demonstrated in living patients with material derived from carotid, coronary and renal distal protection devices, demonstrating the presence of oxidized lipids in clinically relevant lesions(34).

Limitations

Although the similar imaging efficacy was observed in two atherosclerotic mouse strains, the current study did not specifically image vulnerable plaques. Dedicated toxicology studies will be needed to formally test the safety of the current targeted manganese nanoparticles. Due to limitations in the current study design it was not possible to evaluate the mechanism of uptake of the targeted micelles in intraplaque macrophages. Future studies are planned in macrophages scavenger receptor (MSR) knockout mice to evaluate the effect of macrophage phenotype on intracellular uptake. Additionally, the current study used extreme in vitro conditions to evaluate transmetallation. Since other cations as well as endogenous proteins and macromolecules may influence transmetallation, these studies will be repeated using more in vivo physiologic conditions. Additionally, direct methods such as ICP-HPLC will be used to evaluate the in vivo concentration of metabolites that are indicative of transmetallation (ZnDTPA, CuDTPA, CaDTPA).

Conclusions

The current study demonstrates the use of novel bio-compatible Mn molecular imaging probes for the in vivo detection of OSE within atherosclerotic lesions. These observations support the concept that active targeting of Mn to OxLDL rich intraplaque macrophages/ foam cells will allow for sensitive and robust in vivo detection and monitoring of high-risk atherosclerotic lesions.

Supplementary Material

Refer to Web version on PubMed Central for supplementary material.

Acknowledgments

This investigation was supported by the Fondation Leducq (ST, JLW) and by the NIH (R21 HL091399, Briley-Saebo (PI).

References

1. Virmani R, Burke AP, Farb A, Kolodgie FD. Pathology of the vulnerable plaque. J Am Coll Cardiol. 2006; 47:C13–C18. [PubMed: 16631505]
2. Tsimikas S, Brilakis ES, Miller ER, et al. Oxidized phospholipids, Lp(a) lipoprotein, and coronary artery disease. N Engl J Med. 2005; 353:46–57. [PubMed: 16000355]
3. Tsimikas S, Miller YI. Oxidative modification of lipoproteins: mechanisms, role in inflammation and potential clinical applications in cardiovascular disease. Curr Pharma Des. 2011; 17:27–37.
4. Kiechl S, Willeit J, Mayr M, et al. Oxidized phospholipids, lipoprotein(a), lipoprotein-associated phospholipase A2 activity, and 10-year cardiovascular outcomes: prospective results from the Bruneck study. Arterioscler Thromb Vasc Biol. 2007; 27:1788–95. [PubMed: 17541022]
5. Briley-Saebo KC, Shaw PX, Mulder WJ, et al. Targeted molecular probes for imaging atherosclerotic lesions with magnetic resonance using antibodies that recognize oxidation-specific epitopes. Circulation. 2008; 117:3206–15. [PubMed: 18541740]
6. Briley-Saebo KC, Cho YS, Shaw PX, et al. Targeted iron oxide particles for in vivo magnetic resonance detection of atherosclerotic lesions with antibodies directed to oxidation-specific epitopes. J Am Coll Cardiol. 2011; 57:337–47. [PubMed: 21106318]
7. Bartolini ME, Pekar J, Chettle DR, et al. An investigation of the toxicity of gadolinium based MRI contrast agents using neutron activation analysis. Magn Reson Imaging. 2003; 21:541–544. [PubMed: 12878264]
8. Ide M, Kuwamura M, Kotani T, Sawamoto O, Yamate J. Effects of gadolinium chloride (GdCl(3)) on the appearance of macrophage populations and fibrogenesis in thioacetamide-induced rat hepatic lesions. J Comp Pathol. 2005; 133:92–102. [PubMed: 15964588]
9. Sieber MA, Steger-Hartmann T, Lengsfeld P, Pietsch H. Gadolinium-based contrast agents and NSF: evidence from animal experience. J Magn Reson Imaging. 2009; 30:1268–1276. [PubMed: 19938039]
10. Eser G, Karabacakoglu A, Karakose S, Eser C, Kayacetin E. Mangafodipir trisodium-enhanced magnetic resonance imaging for evaluation of pancreatic mass and mass-like lesions. World J Gastroenterol. 2006; 12:1603–1606. [PubMed: 16570354]
11. Toft KG, Hustvedt SO, Grant D, Friisk GA, Skotland T. Metabolism of mangafodipir trisodium (MnDPDP), a new contrast medium for magnetic resonance imaging, in beagle dogs. Eur J Drug Metab Pharmacokinet. 1997; 22:65–72. [PubMed: 9179562]
12. Nordhoy W, Anthonsen HW, Bruvold M, et al. Intracellular manganese ions provide strong T1 relaxation in rat myocardium. Magn Reson Med. 2004; 52:506–514. [PubMed: 15334568]
13. Nordhoy W, Anthonsen HW, Bruvold M, Jynge P, Krane J, Brurok H. Manganese ions as intracellular contrast agents: proton relaxation and calcium interactions in rat myocardium. NMR Biomed. 2003; 16:82–95. [PubMed: 12730949]
14. Koenig SH, Baglin C, Brown RD. Magnetic-Field Dependence of Solvent Proton Relaxation Induced by Gd3+ and Mn2+ Complexes. Magn Reson Med. 1984; 1:496–501. [PubMed: 6443784]
15. Tsimikas S, Palinski W, Halpern SE, Yeung DW, Curtiss LK, Witztum JL. Radiolabeled MDA2, an oxidation-specific, monoclonal antibody, identifies native atherosclerotic lesions in vivo. J Nucl Cardiol. 1999; 6:41–53. [PubMed: 10070840]
16. Tsimikas S, Shortal BP, Witztum JL, Palinski W. In vivo uptake of radiolabeled MDA2, an oxidation-specific monoclonal antibody, provides an accurate measure of atherosclerotic lesions

rich in oxidized LDL and is highly sensitive to their regression. Arterioscler Thromb Vasc Biol. 2000; 20:689–97. [PubMed: 10712392]

17. Jung JH, An K, Kwon OB, Kim HS, Kim JH. Pathway-specific alteration of synaptic plasticity in Tg2576 mice. Molecules and Cells. 2011
18. Dei R, Takeda A, Niwa H, et al. Lipid peroxidation and advanced glycation end products in the brain in normal aging and in Alzheimer's disease. Acta Neuropathol(Berl). 2002; 104:113–122. [PubMed: 12111353]
19. Lauffer RB, Vincent AC, Padmanabhan S, et al. Hepatobiliary MR contrast agents: 5-substituted iron-EHPG derivatives. Magn Reson Med. 1987; 4:582–590. [PubMed: 3613958]
20. Mulder WJ, Koole R, Brandwijk RJ, et al. Quantum dots with a paramagnetic coating as a bimodal molecular imaging probe. Nano Lett. 2006; 6:1–6. [PubMed: 16402777]
21. Lauffer RB. Paramagnetic Metal-Complexes as Water Proton Relaxation Agents for Nmr Imaging - Theory and Design. Chemical Reviews. 1987; 87:901–927.
22. Bruvold M, Nordhoy W, Anthonsen HW, Brurok H, Jynge P. Manganese-calcium interactions with contrast media for cardiac magnetic resonance imaging: a study of manganese chloride supplemented with calcium gluconate in isolated Guinea pig hearts. Invest Radiol. 2005; 40:117–125. [PubMed: 15714086]
23. Rovetta F, Catalani S, Steimberg N, et al. Organ-specific manganese toxicity: a comparative in vitro study on five cellular models exposed to MnCl(2). Toxicol In Vitro. 2006
24. Khan KN, Andress JM, Smith PF. Toxicity of subacute intravenous manganese chloride administration in beagle dogs. Toxicol Pathol. 1997; 25:344–50. [PubMed: 9280117]
25. Rongved, P.; Karlson, JO.; Briley Saebo, K. Amersham, assignee. Magnetic Resonance Imaging Method and Compounds For Use in the Method. US patent. US2006/023529A1. 2006.
26. Zhu D, Lu XL, Hardy PA, Leggas M, Jay M. Nanotemplate-engineered nanoparticles containing gadolinium for magnetic resonance imaging of tumors. Invest Radiol. 2008; 43:129–140. [PubMed: 18197065]
27. Weinreb JC, Abu-Alfa AK. Gadolinium-based contrast agents and nephrogenic systemic fibrosis: why did it happen and what have we learned? J Magn Reson Imaging. 2009; 30:1236–1239. [PubMed: 19938035]
28. Larsen LE, Grant D. General toxicology of MnDPDP. Acta radiologica. 1997; 38:770–9. [PubMed: 9245973]
29. Torzewski M, Shaw PX, Han KR, et al. Reduced in vivo aortic uptake of radiolabeled oxidation-specific antibodies reflects changes in plaque composition consistent with plaque stabilization. Arterioscler Thromb Vasc Biol. 2004; 24:2307–12. [PubMed: 15528482]
30. Spencer A, Wilson S, Harpur E. Gadolinium chloride toxicity in the mouse. Hum Exp Toxicol. 1998; 17:633–637. [PubMed: 9865421]
31. Briley-Saebo KC, Cho YS, Tsimikas S. Imaging of oxidation-specific epitopes in atherosclerosis and macrophage-rich vulnerable plaques. Curr Cardiovasc Imaging Rep. 2011; 4:4–16. [PubMed: 21297859]
32. Tang TY, Muller KH, Graves MJ, et al. Iron oxide particles for atheroma imaging. Arterioscler Thromb Vasc Biol. 2009; 29:1001–1008. [PubMed: 19229073]
33. Trivedi RA, JMUK-I, Graves MJ, et al. In vivo detection of macrophages in human carotid atheroma: temporal dependence of ultrasmall superparamagnetic particles of iron oxide-enhanced MRI. Stroke. 2004; 35:1631–5. [PubMed: 15166394]
34. Ravandi A, Harkewicz R, Leibundgut G, et al. Identification of oxidized phospholipids and cholesteryl esters in embolic protection devices post percutaneous coronary, carotid and peripheral interventions in humans. Arterioscler Thromb Vasc Biol. 2011:P385.

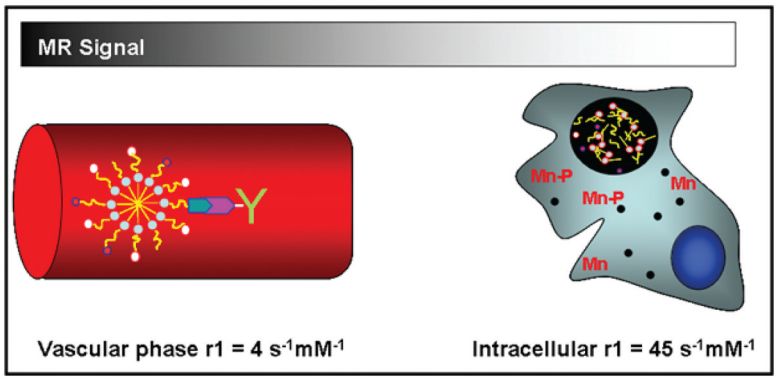

Figure 1.
Diagram of the efficacy of OxLDL targeted Mn micelles in the vascular phase. Mn is chelated to DTPA. Mn is released with the endosomes/lysosomes after uptake into intraplaque macrophage/foam cells (black circle). Due to intracellular release of Mn and subsequent interaction with intracellular components the MR signal is greatly enhanced. The r1 values are derived from Table 2.

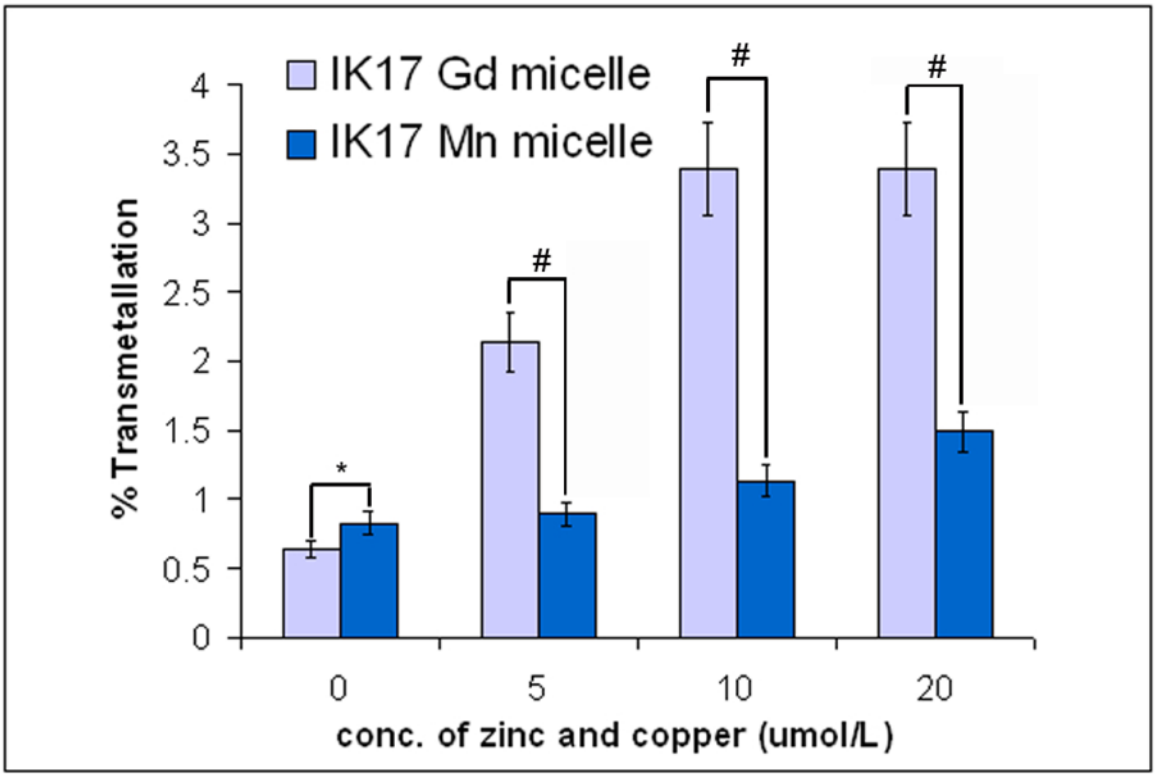

Figure 2.
Percent transmetallation of IK17 labeled Mn(II) and Gd(III) micelles after exposure to copper and zinc. All samples were prepared in 2% BSA and the percent transmetallation determined using relaxometry methods. *=$p<0.05$, #=$p<0.01$ represents Mann-Whitney test for differences between groups at each condition.

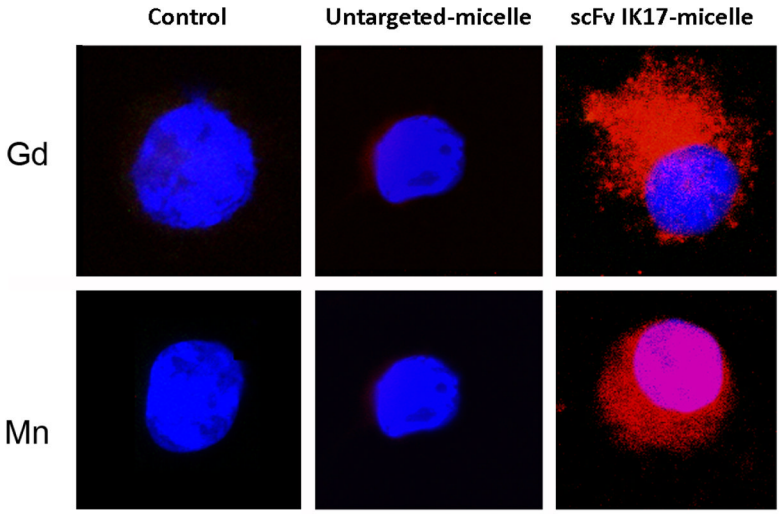

Figure 3.
Confocal imaging of activated J774A.1 macrophages 24 hours after incubation with untargeted and IK17 labeled Mn(II) and Gd(III) micelles. All cell nuclei were DAPI labeled (blue) and all micelles were rhodamine labeled (red).

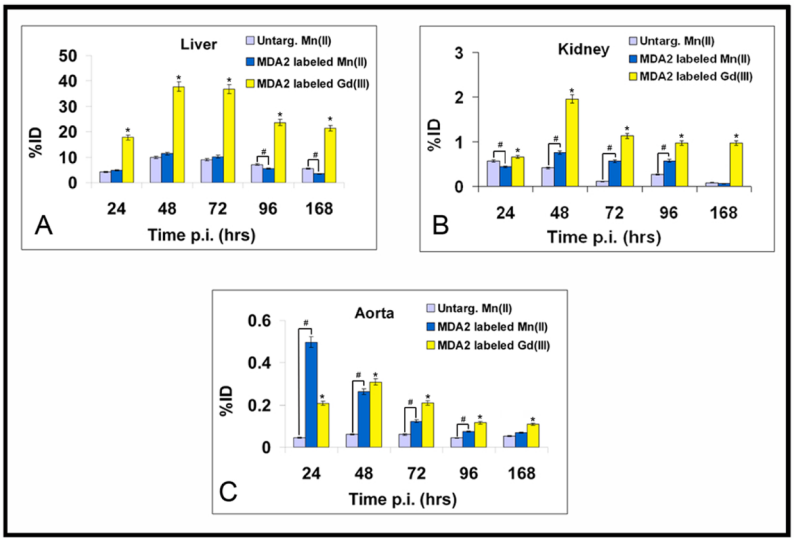

Figure 4.

Biodistribution of untargeted Mn(II) micelles, MDA2 labeled Mn(II) micelles and Gd(III) micelles the liver (A), kidney (B) and aorta (C) of apoE−/− mice. Dosages of 0.05 mmol/Kg and 0.075 mmol/Kg Mn(II) and Gd(III) were administered, respectively. The percent injected doses (%ID) were determined based upon the wet weight of the tissue. Kruskal-Wallis test was used to assess differences between the 3 types of micelles. #=$p<0.05$ comparing untargeted and MDA2 labeled Mn(II) formulations. *=$p<0.05$ comparing MDA2-Mn and MDA2-Gd micelles.

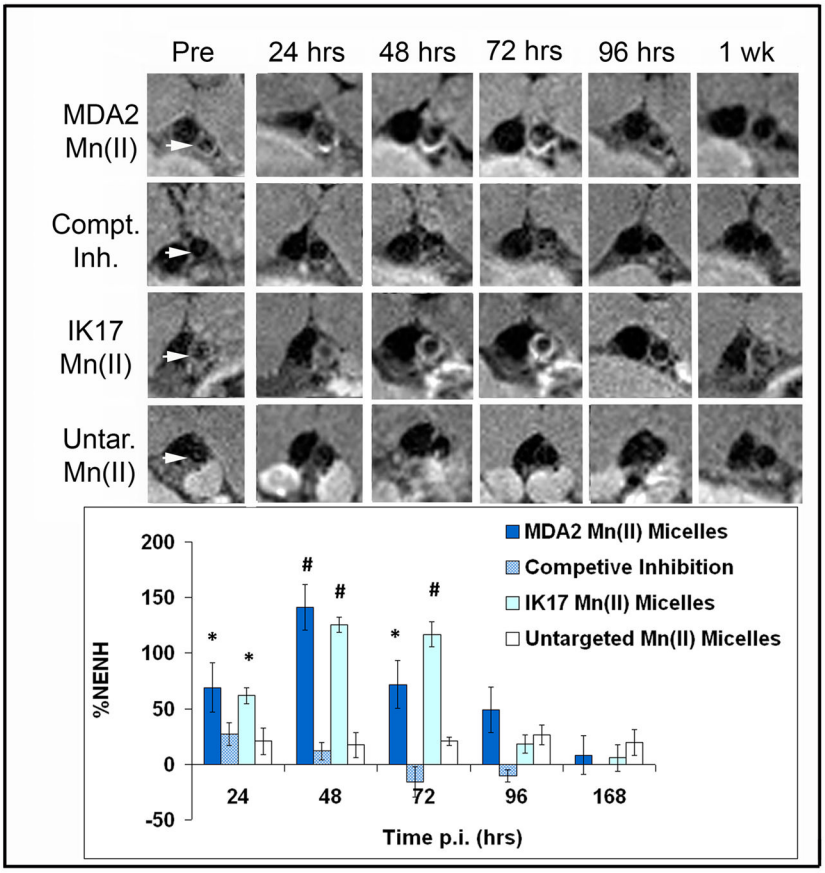

Figure 5.

Representative MR images obtained in the abdominal aorta (white arrows) of apoE−/− mice following injection of Mn micelles (0.05 mmol Mn/Kg). The percent normalized enhancement values (%NENH) represents the relative change in the contrast-to-noise ratios pre and post imaging. For the competitive inhibition studies, 3 mg of free MDA2 antibody was co-injected with the MDA2 labeled Mn micelles. used to compare the 4 types of micelles. *=$p<0.05$, #=$p<0.01$ represents Kruskal–Wallis tests for differences between groups compared to the untargeted Mn micelles.

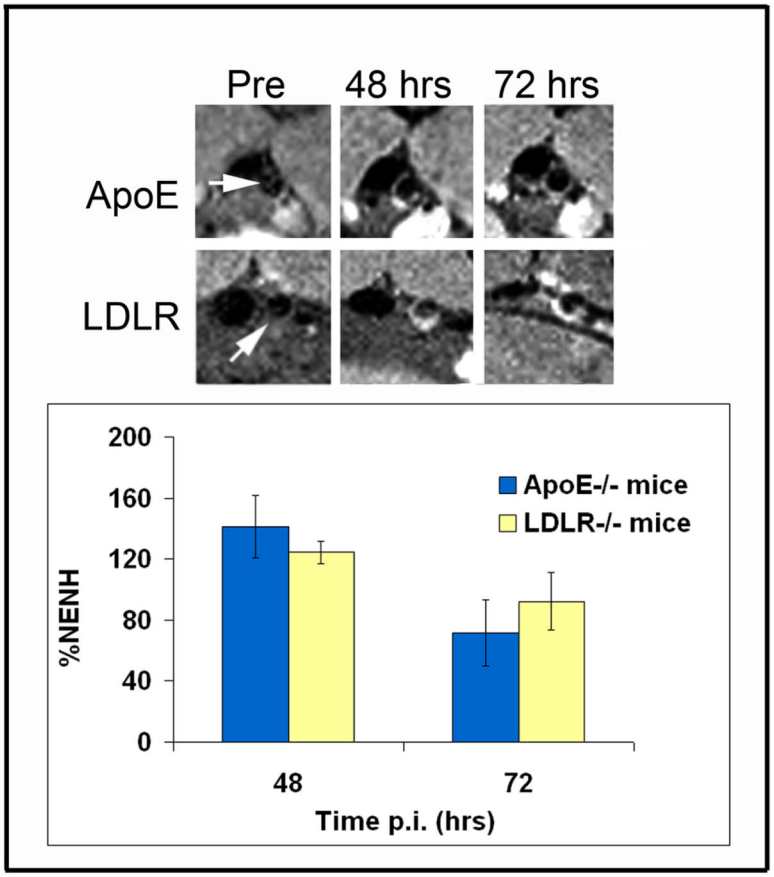

Figure 6.

Representative MR imaging of apoE−/− and LDLR−/− mice 48 and 72 hours after administration of MDA2 labeled Mn micelles. No significant differences were noted between groups using the Mann-Whitney test

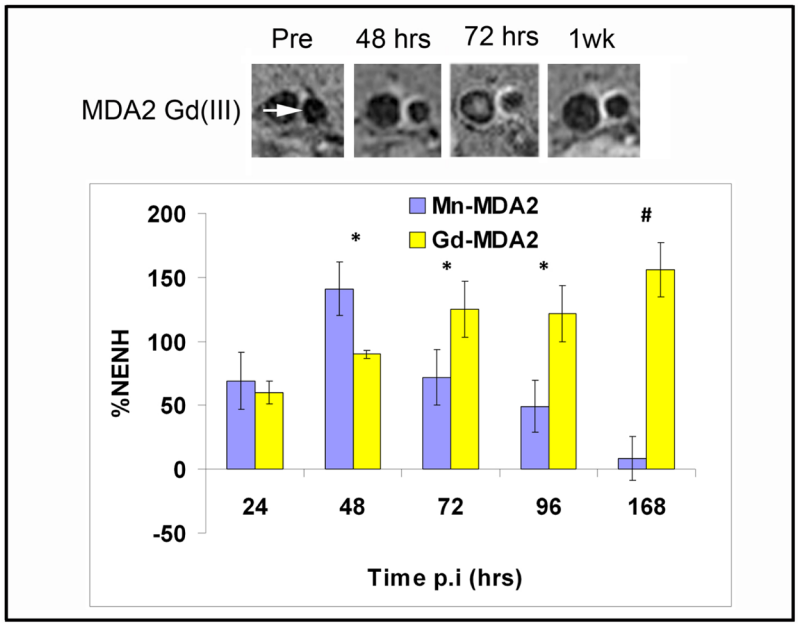

Figure 7.
Comparison of MDA2 labeled Gd and Mn micelles in apoE−/− mice. Mice were administered 0.075 mmol/Kg and 0.05 mmol/Kg Gd and Mn, respectively. *=p<0.05, #=p<0.01 represents Mann-Whitney test for differences between groups at each timepoint.

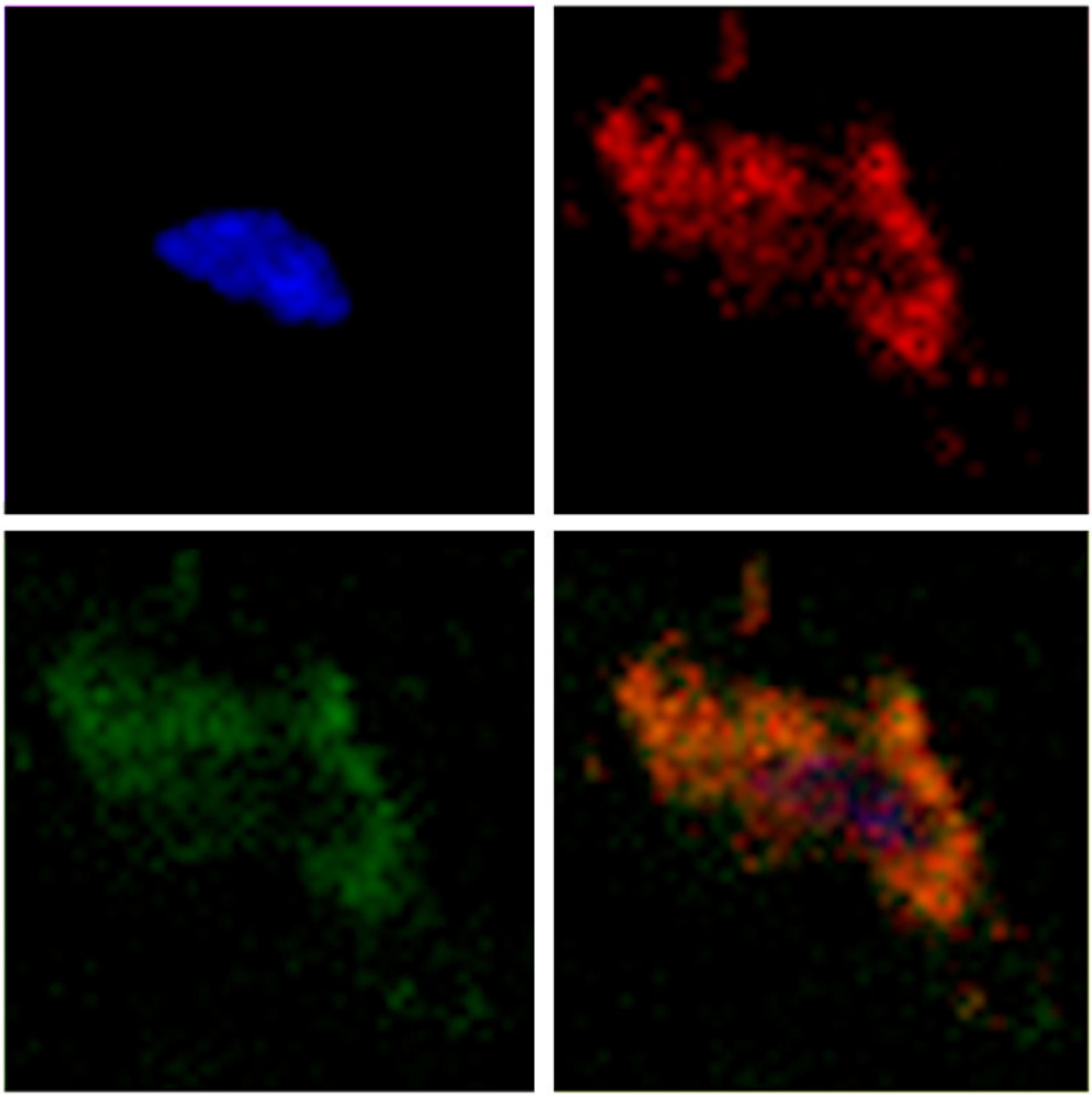

Figure 8.
Confocal microscopy of obtained in the abdominal arterial wall of an apoE−/− mouse 48 hours after administration of MDA2 labeled Mn micelles. Cell nuclei were stained with DAPI (Blue, upper left corner), micelles were labeled with rhodamine (red, upper left corner), macrophages were RPE-labeled anti-CD68 (green, lower left corner). The composite image of all channels is shown in the bottom right corner.

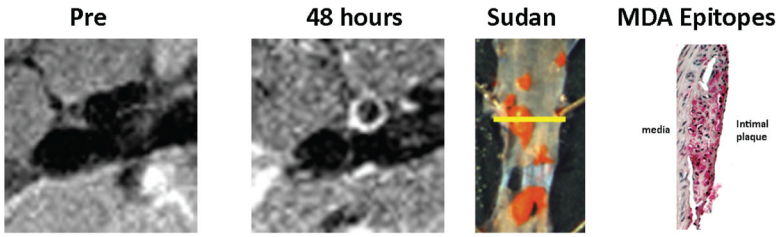

Figure 9.

Representative correlation between in vivo MRI and the presence of MDA epitopes. The aorta was imaged in vivo prior to and 48 hours after the administration of 0.05 mmol Mn/Kg MDA2 labeled micelles. The mouse was sacrificed immediately after imaging and the immunohistology performed. The aorta was opened longitudinally and stained with Sudan (red color). The yellow line in the Sudan stained aorta reflects the area of MR imaging and histological assessment for MDA epitopes. Strong MR signal was observed in regions exhibiting plaque deposition and the presence of MDA-lysine epitopes (red).

Table 1

Overview of all in vivo studies

Study	Description	# apoE−/− mice	# LDLR−/− mice	# WT mice
pKa	Blood drawn over a 24 hour time period in n=3/formulation. Untargeted, MDA2 and IK17 Mn(II) formulations tested	9		9
Biodistribution	Tissue excised after 24, 48, 72, 96 and 1 wk injection. N=3 formulation/time point. Untargeted, MDA2 and IK17 Mn(II) formulations tested.	45		
Neurotoxicity	MR imaging and brain uptake of targeted and MDA2 micelles (n=3/formulation)	6		
MR Imaging in apoE−/− mice	MR imaging performed over a 1 wk time interval post injection (n=8/formulation). Untargeted, MDA2 and IK17 Mn(II) formulations tested. MDA2 Gd (III) micelles re-tested.	32		
Competitive inhibition	MR imaging performed over a 1 wk time interval post injection (n=3/formulation). Only MDA2 Mn(II) formulation tested.	3		
MR Imaging in LDLR−/− mice	MR imaging performed over a 1 wk time interval post injection (n=8/formulation). Only untargeted and MDA2 Mn(II) formulations tested.		16	

Table 2

Physical properties, relaxivities and half-life of the various micelles

Formulation	Size < d>n± SD (nm)	r1, 60 MHz Buffer ($s^{-1}mM^{-1}$)	r1, 60 MHz WT blood ($s^{-1}mM^{-1}$)	r1, 60 MHz apoE−/− blood ($s^{-1}mM^{-1}$)	r1, 60 MHz J744A.1 Intracellular ($s^{-1}mM^{-1}$)	t1/2 hours
Untargeted Mn(II)	10 ± 2	4.1 ± 0.2	3.9 ± 0.4	4.2 ± 0.3	< DL	3.4*
Untargeted Gd(III)	14 ± 2	11.6 ± 0.3	10.5 ± 0.4	10.8 ± 0.4	-	1.5
MDA2 labeled Mn(II)	18 ± 3	4.1 ± 0.2	3.9 ± 0.3	8.1 ± 0.4#	45 ± 5	16.4*
MDA2 labeled Gd(III)	22 ± 2	9.8 ± 0.3	10.6 ± 0.2	12.6 ± 0.2#	-	14.3
IK17- Mn	12 ± 2	3.8 ± 0.2	3.6 ± 0.4	8.2 ± 0.4#	-	12.3*
IK17- Gd	16 ± 3	10.5 ± 0.3	10.6 ± 0.3	12.6 ± 0.3#	-	-

<d>n is the hydrated particle diameter (number weighting). The longitudinal relaxivities (r1) were determined at 60 MHz and 40° C in buffer, wild type mouse blood (WT), and apoE−/− mouse blood. Blood half-lives (t1/2) were obtained in apoE−/− mice following administration of 0.05 mmol/Kg or 0.075 mmol/kg Mn(II) and Gd(III) micelles, respectively.

* = multi-exponential decay observed.

= significant ($p<0.01$) difference in the r1 values observed in WT mouse blood versus apoE−/− mouse blood.